Turkish Journal of Electrical Engineering & Computer Sciences

http://journals.tubitak.gov.tr/elektrik/

Research Article

Turk J Elec Eng & Comp Sci
(2016) 24: 2163 – 2173
© TÜBİTAK
doi:10.3906/elk-1402-45

# Gain and coherence collapse condition for a laser diode with optoelectronic feedback using Volterra series

**Remzi YILDIRIM, Hüseyin CANBOLAT***
Electrical and Electronics Engineering Department, Faculty of Engineering and Nature Sciences,
Yıldırım Beyazıt University, Ankara, Turkey

**Received:** 05.02.2014 • **Accepted/Published Online:** 05.07.2014 • **Final Version:** 15.04.2016

**Abstract:** Four-tone small signal analysis was performed for a nonlinear optoelectronic feedback laser diode system. In the analysis, Volterra power series up to second-order opening, the second kernel for the output intermodulation distortion (IMD) analysis was performed. The components of the alternative IMD frequency were selected for analysis. These are the four IMD frequency components. The variation of IMD frequency component amplitudes was investigated under various values of delay-time ($t_0$) and the feedback gain constant ($K$). The feedback values and the critical frequencies, at which the coherence collapse or chaos occur, were also determined.

**Key words:** Laser diode, Volterra series, intermodulation, harmonic distortion, nonlinear distortion, electronics feedback, chaos, gain, nonlinear optoelectronic feedback

## 1. Introduction

Laser systems, which are the optical source for fibre-optic and hybrid communication systems, employ various laser diode applications. Laser diodes have been increasingly used both commercially and industrially due to their optical characteristics, small size, and ruggedness. Laser diodes have three main characteristic quantities: gain [1–3], refractive index change [4–6], and linewidth enhancement factor [7–9]. These quantities have been studied many times theoretically [10–15], experimentally [16–24], and intelligently [22–42]. In this current study, the characteristic quantity gain and coherence collapse condition with optoelectronic feedback are analysed and simulated with the use of Volterra series.

In optical communication systems, different optical feedback schemes are used based on the structure of the laser diode. Hybrid (analogue/digital) communication system structures for metropolitan areas consist of fibre-optic and coaxial cables and use feedback for different purposes [43]. In recent years, data communication is widely used due to extensive use of the Internet. However, the communication systems infrastructure has reached its limits to meet this fast increasing demand for data transfer. To overcome this problem, the bandwidth of systems can be increased with the use of subcarrier systems. The prominent property of these systems is the use of the wideband subcarrier multiplexing (SCM) technique. SCM systems are classified according to the employed analogue and digital modulation techniques. Asymmetric digital subcarrier line (ADSL), digital subcarrier line (DSL), very-high speed digital subcarrier line (VDSL), discrete multitone (DMT), discrete wavelet multitone (DWMT), and wavelength division multiplexing (WDM) are some examples of SCM systems. Due to the nonlinear behaviour of laser diodes, intermodulation distortion (IMD) frequency components are generated.

*Correspondence: huseyin.canbolat@gmail.com

The systematic analysis of Volterra kernels is carried out in [44]. Several authors presented results on harmonic distortion, optimised intermodulation [45–49,50,51], and various aspects of the issue [52,53].

The use of an optic filter system in optical feedback provides the stable operation of the dynamic system by controlling the nonlinear transmission function through the filter [54]. Moreover, the operation of the dynamic system can be adjusted by means of the feedback systems [55]. Feedback is also used in controlling the dynamic systems with various modulation types [56–58]. Another use of feedback is to achieve wavelength stability [59] of wavelength division multiplexing (WDM) systems through the adjustment of cross-correlation level by setting up the DC bias current [60].

In high speed fibre-optic systems, chaotic laser systems are used. The properties of chaotic communication systems change depending on bandwidth, performance, bit error rate, and the length of the fibre-optic line [61]. Rotated polarisation and inverted polarisation optical feedback systems are used in chaos-based safe fibre-optic communication systems [62]. Adjustable time delayed optoelectronic feedback is used in safe chaos-based multiplexed communication systems [63,64]. The feedback between nonlinear elliptical polarisation and laser source is another optical feedback method [65]. Feedback is used for steady data transmission in commercial communication systems [66]. For high resolution two-tone separation and two-tone signal quality, an optical filter/feedback system is used [67]. Feedback methods are also used for setting the quality factor, gain, and loss [68]. For dynamic systems, time delayed polarisation mode switching in semiconductor lasers polarisation rotating coupling methods are applied [69]. In nonlinear dynamic delayed feedback optoelectronic oscillator systems, dual fibre optical feedback is used between the hybrid system and the oscillator [70]. In another study, the stability of the feedback system is achieved by the relaxation oscillation frequency feedback current [71]. Periodical feedback oscillation is obtained by high injection current [72]. The coherence collapse regime is used to focus the optical output power and the reflected optical power under test [73].

In this work, the analysis of alternative IMD frequency components of a nonlinear laser diode with optoelectronic feedback under four-tone small signal input is performed. The Volterra operators $Z_1$, $Z_2$ and the Volterra kernels $H_1$, $H_2$ are found. The analysis is carried out for the second kernel output.

The main contribution this study is that alternative IMD frequency components are employed in order to increase the bandwidth of the fibre-optic system.

## 2. The basic single-mode laser diode

Hassine [74], Tucker [75], and Olshansky [76] modelled the basic single mode laser diode using the following dynamic equations:

$$\frac{dp(t)}{dt} = \Gamma A\left[n(t) - N_{tr}\right]\left[1 - \hat{\varepsilon}p(t)\right]p(t) - \frac{1}{\tau_p}p(t) + \frac{\beta\Gamma}{\tau_n}n(t) \tag{1}$$

$$\frac{dn(t)}{dt} = \frac{1}{q}I(t) - \frac{1}{\tau_n}n(t) - \Gamma A\left[n(t) - N_{tr}\right]\left[1 - \hat{\varepsilon}p(t)\right]p(t), \tag{2}$$

where $p(t)$ and $n(t)$ denote the photon and carrier numbers, respectively, and $\Gamma$ the compression factor ($\Gamma = 0.3$), $A$ gain constant ($A = 1.83\ times\ 10^4 \mathrm{s}^{-1}$), $N_{tr}$ the number of carriers at the threshold ($N_{tr} = 10^7$), $\tau_p$ photon life ($\tau_p = 1.6\ times\ 10^{-12}\mathrm{s}$), $\tau_n$ carrier life ($\tau_n = 2.2\ times\ 10^{-9}\mathrm{s}$), $\beta$ spontaneous emitting factor ($\beta = 10^{-4}$), $I(t)$ total current, $q$ elementary charge ($q = 1.6\ times\ 10^{-19}\mathrm{C}$), $\hat{\varepsilon} = \varepsilon/V = 1 \times 10^{-6}$ dimensionless gain factor, and $V$ the volume of the active region.

Using (1) and (2), the Volterra kernels ($H_1$, $H_2$) are determined. The interested reader is referred to [66–70] for details of Volterra and the nonlinear system theories and to [44] for the detailed solutions of a single-mode laser diode.

In [45,46], the analysis of the system with two-tone and three-tone inputs for the harmonic distortion, the bandwidth, and the optimisation is given with the results. The general four-tone small signal input $i(t)$ is given as

$$\begin{aligned} i(t) &= u_o \cos(\omega_o t + \delta_0) + u_1 \cos(\omega_1 t + \delta_1) + u_2 \cos(\omega_2 t + \delta_2) \\ &\quad + u_3 \cos(\omega_3 t + \delta_3) + u_4 \cos(\omega_4 t + \delta_4) \end{aligned}, \tag{3}$$

where $u_i$, $\omega_i$, and $\delta_i$ are the amplitude, frequency, and phase of the *ith* ($i$ = 1,2,3,4) input, respectively. The carrier signal is represented by $u_o \cos(\omega_o t + \delta_o)$. The number of photons, $P(t)$, at the output is given as

$$P(t) = p_1(t) + p_2(t) + p_3(t) + .... + p_n(t) = \sum_{i=1}^{n} p_i(t), \tag{4}$$

where $p_i(t)$ ($i$ = 1,2,...,n) is the estimated photon numbers of the *ith* Volterra kernel [44,45].

## 3. The first-order Volterra operator

The transfer function $Z_1(j\omega)$ of the first order Volterra operator is given as [44]

$$Z_1(j\omega) = \frac{H_1(j\omega)}{1 + H_1(j\omega)G_1(j\omega)}, \tag{5}$$

where $H_1(j\omega)$ and $G_1(j\omega)$ is defined as

$$H_1(j\omega) = \frac{B_o}{q}\left(\frac{1}{(D_o - \omega^2) + jD_1\omega}\right) \tag{6}$$

$$G_1(j\omega) = ge^{-j\omega t_o}, \tag{7}$$

where $B_0$, $D_0$ and $D_1$, and $g$ are constants and $t_0$ is the normalised time. The detailed definitions can be found in [44].

The input current, $i(t)$, is selected as in (3) excluding carrier component as follows:

$$i(t) = u_1 \cos(\omega_1 t + \delta_1) + u_2 \cos(\omega_2 t + \delta_2) + u_3 \cos(\omega_3 t + \delta_3) + u_4 \cos(\omega_4 t + \delta_4). \tag{8}$$

The photon output of the first order Volterra kernel is defined as

$$\begin{aligned} p_1 &= u_1 |Z_1(j\omega_1) \cos[\omega_1 t + \delta_1 + \angle Z_1(j\omega_1)]| + u_2 |Z_1(j\omega_2) \cos[\omega_2 t + \delta_2 + \angle Z_1(j\omega_2)]| \\ &\quad + u_3 |Z_1(j\omega_3) \cos[\omega_3 t + \delta_3 + \angle Z_1(j\omega_3)]| + u_4 |Z_1(j\omega_3) \cos[\omega_4 t + \delta_4 + \angle Z_1(j\omega_4)]| \end{aligned}, \tag{9}$$

where $|Z_1(j\omega_i)|$, $\angle Z_1(j\omega_i)$ and $\omega_i$ ($i$ = 1,2,3,4) denote the amplitude, phase, and the angular frequencies of the input currents, respectively.

## 4. The second-order Volterra operator

Using the block diagrams given in [44], the block diagram of the second order Volterra operator, $p_2(t)$, can be obtained as given in Figure 1.

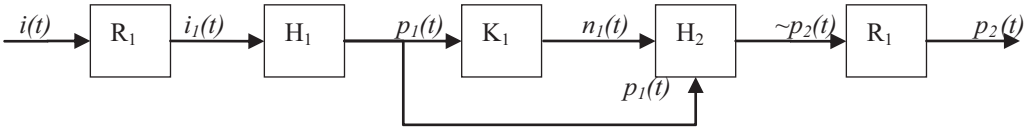


**Figure 1.** Block diagram of the second-order Volterra operator.

In Figure 1, the $R_1$ and $H_1$ are linear time invariant (LTI) systems. The $R_1$ block is defined in terms of $G_1$ and $H_1$ given in (6) and (7), respectively, as

$$R_1(j\omega) = \frac{1}{1 + H_1(j\omega) G_1(j\omega)} \tag{10}$$

Since $R_1$ and $H_1$ blocks are connected in series, the equivalent block has the following transfer function:

$$R_1(j\omega) H_1(j\omega) = \frac{H_1(j\omega)}{1 + H_1(j\omega) G_1(j\omega)}. \tag{11}$$

The photon output is in the following form:

$$p_1(t) = A_1 \cos(\omega_1 t + \alpha_1) + A_2 \cos(\omega_2 t + \alpha_2) + A_3 \cos(\omega_3 t + \alpha_3) + A_4 \cos(\omega_4 t + \alpha_4), \tag{12}$$

where

$$A_i = u_i |Z_1(j\omega_i)| \, (i = 1, 2, 3, 4) \tag{13a}$$

$$\alpha_i = \delta_i + \angle Z_1(j\omega_i) \, (i = 1, 2, 3, 4). \tag{13b}$$

The carrier density, $n_1(t)$, has the following form:

$$n_1(t) = B_1 \cos(\omega_1 t + \beta_1) + B_2 \cos(\omega_2 t + \beta_2) + B_3 \cos(\omega_3 t + \beta_3) + B_4 \cos(\omega_4 t + \beta_4) \tag{14}$$

The $K_1$ block has the following transfer function [44]:

$$K_1(j\omega) = \frac{1}{B_o}(B_1 + j\omega), \tag{15}$$

where

$$B_i = A_i |K_1(j\omega_i)| \, (i = 1, 2, 3, 4) \tag{16a}$$

$$\beta_i = \alpha_i + \angle K_1(j\omega_i) \, (i = 1, 2, 3, 4). \tag{16b}$$

The block diagram for $H_2$ is given in [44]. To find the output of $H_2$, $p_1^2(t)$ and $n_1(t)p_1(t)$ should be available. From (12),

$$p_1^2(t) = [A_1 \cos(\omega_1 t + \alpha_1) + A_2 \cos(\omega_2 t + \alpha_2) + A_3 \cos(\omega_3 t + \alpha_3) + A_4 \cos(\omega_4 t + \alpha_4)]^2 \tag{17}$$

and from (12) and (14)

$$\begin{aligned} n_1(t)\,p_1(t) &= (A_1\cos(\omega_1 t+\alpha_1)+A_2\cos(\omega_2 t+\alpha_2)+A_3\cos(\omega_3 t+\alpha_3)+A_4\cos(\omega_4 t+\alpha_4)) \\ &\quad (B_1\cos(\omega_1 t+\beta_1)+B_2\cos(\omega_2 t+\beta_2)+B_3\cos(\omega_3 t+\beta_3)+B_4\cos(\omega_4 t+\beta_4)) \end{aligned} \tag{18}$$

are obtained. In [44], $f_2(t)$ is given as

$$f_2(t) = \Gamma A\left[1-2\hat{\varepsilon}P_o\right] n_1(t)\,p_1(t) - \Gamma A\left[N_o - N_{tr}\right] p_1^2(t). \tag{19}$$

The above expression for $f_2(t)$ is obtained by substituting for $p_1^2(t)$ and $n_1(t)p_1(t)$ from (17) and (18).

The function $M(j\omega)$ is given as [44]

$$M(j\omega) = \frac{j\omega - \frac{\beta\Gamma-1}{\tau_n}}{(D_o-\omega^2)+jD_1\omega} R_1(j\omega). \tag{20}$$

Substituting for $R_1$

$$M(j\omega) = \left[\frac{j\omega - \frac{\beta\Gamma-1}{\tau_n}}{(D_o-\omega^2)+jD_1\omega}\right]\left[\frac{D_o-\omega^2+jD_1\omega}{D_o-\omega^2+jD_1\omega+\frac{gB_o}{q}e^{j\omega t_o}}\right] \tag{21}$$

is obtained. The kernel number of photon output $p_2(t)$ is defined as

$$p_2(t) = f_2(t)\,M(0). \tag{22}$$

Substituting $\omega = 0$ in (21), $M(0) = \frac{(1-\beta\Gamma)}{(D_o q+gB_o)}\frac{q}{\tau_n}$. Using this value for $M(0)$, one can obtain the expression for $p_2(t)$ from (22).

The carrier density transfer function is defined as

$$N_2(s) = \frac{1}{B_o}\left[\frac{(s+B_1)\left(s-\frac{\beta\Gamma-1}{\tau_n}\right)}{s^2+D_1 s+D_o} - 1\right] F_2(s). \tag{23}$$

The interested reader is referred to [44,45] for details of the analysis.

## 5. Results

In this study, the input current, $I_0$, is chosen such that $I_0 = 3.33\,I_{th}$. The alternative IMD frequency components, which are obtained from the second kernel output, are chosen as

1. $(\omega_0+\omega_1), (-\omega_0+\omega_1)$,
2. $(\omega_0+\omega_2), (\omega_0-\omega_2)$,
3. $(\omega_0+\omega_3), (\omega_0-\omega_3)$,
4. $(\omega_0+\omega_4), (\omega_0-\omega_4)$.

The results are given in Figures 2–4. The line types indicated in Figure 4 are also valid for Figures 2 and 3.

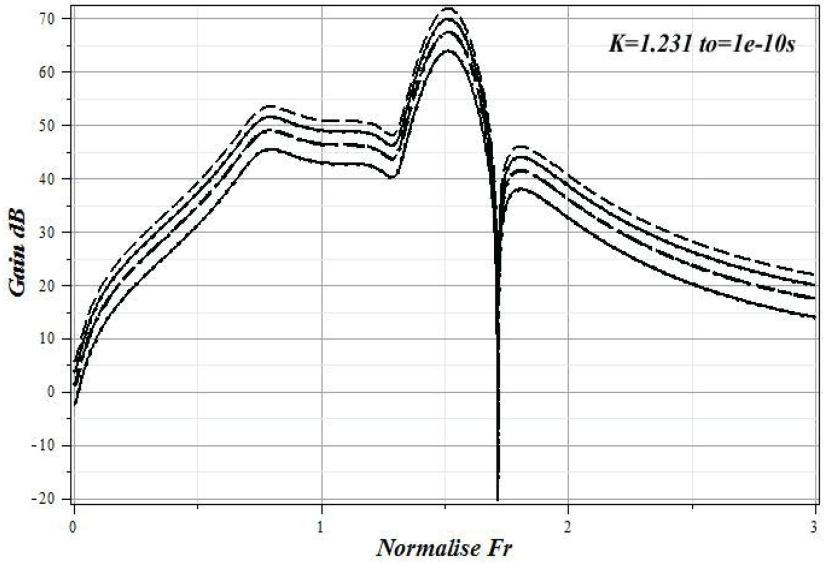


**Figure 2.** Frequency response of the second kernel ($K = 1.231$; $t_0 = 1\ times\ 10^{-10}$s).

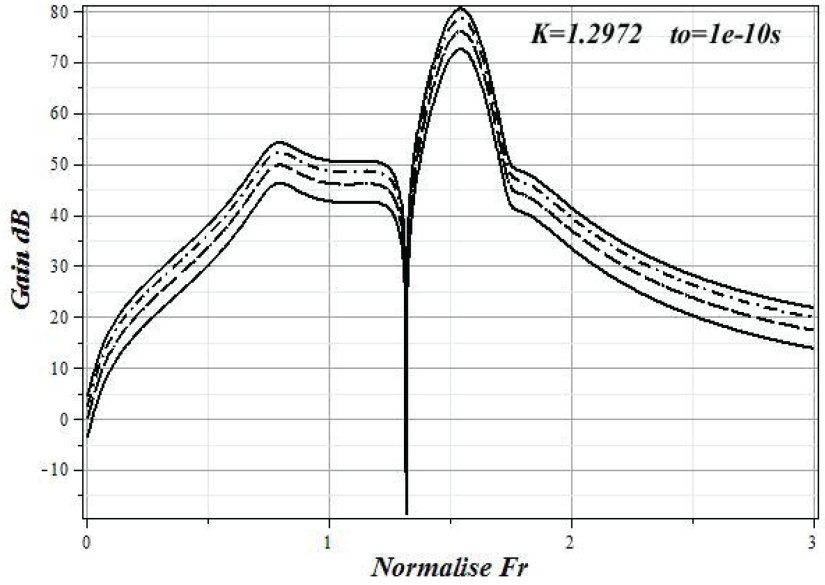


**Figure 3.** Frequency response of the second kernel ($K = 1.2972$; $t_0 = 1\ times\ 10^{-10}$s).

In Figures 2, 3, and 4, the gain curves are given for the feedback gains $K = 1.231$, $K = 1.2972$, and $K = 1.182$ with the delay-time $t_0 = 1\ times\ 10^{-10}$ s. From Figure 2, the bandwidth becomes narrower compared with the analogue and digital communication specifications. However, the gain increases. Here, the normalised collapse frequency value and gain are 1.77 and –21 dB, respectively.

In Figure 3, the normalised collapse frequency and gain are 1.132 and –18.5 dB, respectively, under the feedback gain $K = 1.2972$.

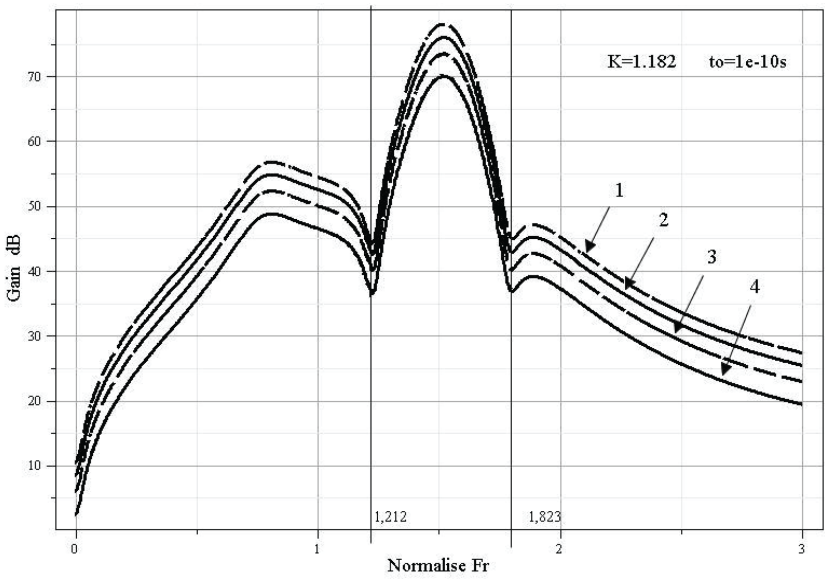


**Figure 4.** Frequency response of the second kernel ($K = 1.182$; $t_0 = 1\ times\ 10^{-10}$s).

In Figure 4 under the feedback gain $K = 1.182$, the normalised collapse frequencies of minimum gain (37.71 dB) are 1.212 and 1.823, and the maximum gain is 79 dB. That is, the optoelectronic system with feedback behaves like a bandpass filter. The bandpass characteristics are found as follows:

$$\omega_L = 1.212_{norm} = 12.12 \text{ GHz}$$

and

$$\omega_H = 1.823_{norm} = 18.23 \text{ GHz},$$

where the *norm* denotes that the value is the normalised frequency value.

This leads the centre frequency to be

$$\omega_0 = \sqrt{\omega_L \omega_H} = 1.486_{norm} = 14.86 \text{ GHz}.$$

Since the bandwidth is

$$BW = \omega_H - \omega_L = 18.23 - 12.12 = 6.11 \text{ GHz},$$

the quality factor or the selectivity $Q = \frac{\omega_0}{BW}$ of the bandpass filter is found as

$$Q = 14.86/6.11 = 2.432[71].$$

Available bandwidths are found as 17.90 GHz and 7.5 GHz for digital and analogue communication, respectively.

## 6. Conclusion

In this study, an optoelectronic feedback system with adjustable gain and time delay is applied to a laser diode. The following is obtained by changing the gain $K$:

The input current is selected as $I_0 = 3.33 I_{th}$. Different $I_0$ values may lead to different results. The normalised frequency at the collapse or chaos corresponding to the critical feedback is found as 1.212 and 1.823. The critical frequency depends on the input current, delay-time, and the feedback gain. Small variations in the feedback can result a chaotic behaviour. The optical system is highly sensitive to variations in the feedback.

The two collapse frequency ranges changed by the ratio of 81.69%, while the change in the input current is 11%. This clearly shows that the system is nonlinear.

An interesting result arises for $K = 1.182$. In this case, the gain curve is very similar to a bandpass filter with low and high bandpass frequencies 12.12 GHz and 18.23 GHz (Figure 4). The centre frequency is estimated as 14.86 GHz with a quality factor larger than 2. However, the gain (37.71 dB) at the low and high frequencies is much higher than $-3$ dB. Additionally, these values change with changing DC injection current.

The critical feedback value for chaos seems impossible to predict. Around the chaos frequencies, the modulation should not be performed. The laser diode systems should be tested for stability at the critical feedback and frequency. Then the system can be employed in fibre-optic subcarrier communication systems.

## References


[1] Chuang SL, Ogorman J, Levi, AFJ. Amplified spontaneous emission and carrier pinning in laser-diodes. IEEE J Quantum Electronics 1993; 29:1631-1639.

[2] Celebi FV. A different approach to gain computation in laser diodes with respect to different number of quantum-wells. Optik 2005; 116: 375-378.

[3] Geels RS, Corzine SW, Coldren LA. Ingaas vertical-cavity surface-emitting lasers. IEEE J Quantum Electronics 1991; 27:1359-1367.

[4] Wenzel H, Erbert G, Enders PM. Improved theory of the refractive-index change in quantum-well lasers. IEEE J Selected Topics in Quantum Electronics 1999; 5:637-642.

[5] Celebi FV, Danisman K. A different approach for the computation of refractive index change in quantum-well diode lasers for different injection levels. Proceedings of SPIE 2004; 5662:384-388. Fifth International Symposium on Laser Precision Microfabrication; Nara; Japan.

[6] Stohs J, Bossert DJ, Gallant DJ. Gain, refractive index change, and linewidth enhancement factor in broad-area GaAs and InGaAs quantum-well lasers. IEEE J Quantum Electronics 2001; 37:1449-1459.

[7] Henry CH. Theory of the linewidth of semiconductor-lasers. IEEE J Quantum Electronics 1982; 18: 259-264.

[8] Celebi FV, Danisman K. Neural estimator to determine alpha parameter in terms of quantum-well number. Optics & Laser Technol 2005; 37:281-285.

[9] Heil T, Fischer I, Elsasser W. Influence of amplitude-phase coupling on the dynamics of semiconductor lasers subject to optical feedback. Physical Review 1999; 60: 634-641.

[10] Uchida T, Miyamoto T, Koyama F. Effect of index variation in active layer on transverse mode for vertical-cavity surface-emitting lasers. Japanese Journal of Applied Physics Part 1-Regular Papers Brief Communications & Review Papers 2006; 45: 2550-2555.

[11] Yildirim R, Celebi FV. The computation of the angle between the gain and photon population by geometrical approach. J Faculty of Eng Architec of Gazi University 2009; 24: 709-714.

[12] Chuang SL. Optical gain of strained wurtzite GaN quantum-well lasers. IEEE J Quantum Electronics 1996; 32:1791-1800.

[13] Fang W, Chuang SL. Theoretical prediction of gan lasing and temperature sensitivity. Applied Physics Letters 1995; 67: 751-753.

[14] Gerhardt NC, Hofmann MR, Hader J. Linewidth enhancement factor and optical gain in (GaIn)(NAs)/GaAs lasers. Applied Physics Letters 2004; 84: 1-3.

[15] Wieczorek S, Krauskopf B, Simpson TB. The dynamical complexity of optically injected semiconductor lasers. Physics Reports-Review Section of Physics Letters 2005; 416: 1-128.

[16] Newell TC, Bossert DJ, Stintz A. Gain and linewidth enhancement factor in InAs quantum-dot laser diodes. IEEE Photonics Technology Letters 1999; 11: 1527-1529.

[17] Yu Y, Giuliani G, Donati S. Measurement of the linewidth enhancement factor of semiconductor lasers based on the optical, feedback self-mixing effect. IEEE Photonics Technology Letters 2004; 16: 990-992.

[18] Su CB, Eom J, Lange CH. Characterization of the dynamics of semiconductor-lasers using optical modulation. IEEE J Quantum Electronics 1992; 28: 118-127.

[19] Xin YC, Li Y, Martinez A. Optical gain and absorption of quantum dots measured using an alternative segmented contact method. IEEE J Quantum Electronics 2006; 42: 725-732.

[20] Walmsley M, Abram RA. Carrier dynamics model of fast refractive index changes in semiconductor laser amplifiers. IEE Proceedings-Optoelectronics 1997; 144: 189-196.

[21] Yucel M, Aslan Z. The noise figure and gain improvement of double-pass C-band EDFA. Microwave and Optical Technol Lett 2013; 55: 2525-2528.

[22] Yucel M, Goktas HH, Ozkaraca O. Temperature dependence of noise figure in the erbium doped fiber amplifier. J Fac Eng Archit Gazi Univ 2010; 25: 635-641.

[23] Yucel M, Goktas HH. Determination of minimum temperature coefficient of C band EDFA. J Applied Sciences 2008; 8: 4464-4467.

[24] Yucel M, Goktaş HH. Design of gain flattenned ultra-wideband hybrid optical amplifier. J Fac Eng Archit Gazi Univ 2007; 22: 863-868.

[25] Ababneh JI, Qasaimeh O. Simple model for quantum-dot semiconductor optical amplifiers using artificial neural networks. IEEE Transactions on Electron Devices 2006; 53: 1543-1550.

[26] Wei Lu, Xi J, Yu Y. Linewidth enhancement factor measurement based on optical feedback self-mixing effect: a genetic algorithm approach. J Optics A-Pure And Applied Optics 2009; 11.

[27] Yucel M. Celebi FV, Goktas HH. Simple and efficient ANN model proposed for the temperature dependence of EDFA gain based on experimental results. Optics And Laser Technology 2013; 45: 488-494.

[28] Roy K. Naskar MK. Genetic evolutionary algorithm for static traffic grooming to SONET over WDM optical networks. Computer Comm 2007; 30: 3392-3402.

[29] Celebi FV, Yucel M, Goktas HH, Danisman K. Intelligent modelling of alpha ($\alpha$) parameter; comparison of ANN and ANFIS cases. Optoelectronics and Advanced Materials, Rapid Communications 2013; 7: 470-474.

[30] Yigit S, Tugrul B, Celebi FV. A complete CAD model for type-I quantum cascade lasers with the use of artificial bee colony algorithm. Journal of Artificial Intelligence 2012; 5: 76-84.

[31] Celebi FV, Yucel M, Goktas HH. Fuzzy logic based device to implement a single CAD model for a laser diode based on characteristic quantities. Optik 2012; 123: 471-474.

[32] Yigit S, Eryigit R, Celebi FV. Optical gain model proposed with the use of artificial neural networks optimised by artificial bee colony algorithm. Optoelectronics and Advanced Materials, Rapid Communications 2011; 5: 1026-1029.

[33] Yucel, M, Goktas, HH, Celebi, FV. Temperature independent length optimization of L-band EDFAs providing flat gain. Optik 2011; 122: 872-876.

[34] Tankiz, S, Celebi FV, Yildirim R. Computer-aided design model for a quantum-cascade laser. IET Circuits, Devices and Systems 2011; 5: 143-147.

[35] Celebi FV, Altindag T. An accurate optical gain model using adaptive neurofuzzy inference system. Optoelectronics and Advanced Materials, Rapid Communications 2009; 3: 975-977.

[36] Celebi FV, Dalkiran I, Danisman K. Injection level dependence of the gain, refractive index variation, and alpha ($\alpha$) parameter in broad-area InGaAs deep quantum-well lasers. Optik 2006; 117: 511-515.

[37] Celebi FV. Modeling of the linewidth enhancement factors of the narrow and wide GaAs well semiconductor lasers. J Faculty of Eng Architec of Gazi University 2006; 21: 161-166.

[38] Celebi FV. A proposed CAD model based on amplified spontaneous emission spectroscopy. J Optoelectronics and Advanced Materials 2005; 7: 1573-1579.

[39] Sagiroglu S, Danisman K. Modelling of the linewidth enhancement factor with the use of radial basis function network. AEU-Archiv fur Elektronik und Ubertragungstechnik 2002; 56: 51-54.

[40] Goktas HH, Yucel M. A fuzzy logic based device for the determination of temperature dependence of EDFAs. Microwave and Optical Technol Lett 2008; 50: 2331-2334.

[41] Yucel M. Fuzzy logic-based automatic gain controller for EDFA. Microwave and Optical Technology Letters 2011; 53: 2703-2705.

[42] Celebi N. A complete type II quantum cascade laser model with the use of RBFN. Optoelectronics and Advanced Materials, Rapid Communications 2013; 7: 188-190.

[43] Lau KY. RF transport over optical fiber in urban wireless infrastructures. J Opt Commun Netw 2012; 4: 326-335.

[44] Schetzen M, Yildirim R. System theory of the single-mode laser-diode. Opt Commun 2003; 219: 341-350.

[45] Schetzen M, Yildirim R. Application of the single–mode laser diode system theory. Opt Commun 2003; 219: 351-355.

[46] Aydin E, Yildirim R. Optimizing the performance of single-mode laser diode system using genetic algorithm. Opt Laser Eng 2004; 42: 41-46.

[47] Yıldırım R. Intermodulation distortion system theory of the three-tone small signal input laser diode with non-linear optoelectronic feedback. J Fac Eng Arch Gazi Univ 2007; 22: 417-430.

[48] Schetzen M, Yildirim R, Çelebi F. Intermodulation distortion of the single-mode laser-diode. Appl Phys B 2008; 93: 837–847.

[49] Yıldırım R. Selection of frequency components for symmetric and asymmetric communication systems. J Fac Eng Arch Gazi Univ 2008, 23: 329-341.

[50] Celebi FV, Yildirim R, Gergerli B, Gokrem L. Alternative intermodulation frequency components. International Conf on App of Information and CommTechnol, AICT 2009; Baku; Azerbaijan.

[51] Celebi FV, Yildirim R. Distortion system theory of the two tone small signal input laser diode. J Faculty of Eng Architec of Gazi University 2005; 20: 373-377.

[52] Yıldırım R, Çelebi FV. Harmonic amplitude control in laser diodes with non-linear feedback. J Fac Eng Arch Gazi Univ 2010; 25: 163-170.

[53] Alifaha S, Idrusa SM, Kassima NM, Shenga NY, Rahmata MF, Greenc RJ. Intermodulation distortion analysis of feedforward linearised laser transmitter employing volterra series approach. Optik 2012; 124: 631-634.

[54] Li N, Pan W, Luo B, Yan L, Zou X, Jiang N, Xiang S. High bit rate fiber-optic transmission using a four-chaotic-semiconductor-laser scheme. IEEE Photonic Tech L 2012; 24: 1072-1074.

[55] Pal V, Suelezer J, Prasa A, Vemuri G, Ghosh R. Semiconductor laser dynamics with two filtered optical feedbacks. In: International Conference on Fiber Optics and Photonics; 9–12 December 2012; Chennai, India. Washington, DC, USA: OSA Lasers & Ultrafast Optics III (W3C).

[56] Kingni ST, Van der Sande G, Gelens L, Erneux T, Danckaert J. Direct modulation of semiconductor ring lasers: numerical and asymptotic analysis. J Opt Soc Am B 2012; 29: 1983-1992.

[57] Li N, Pan W, Yan L, Luo B, Xu M, Tang Y, Jiang N, Xiang S, Zhang Q. Chaotic optical cryptographic communication using a three-semiconductor-laser scheme. J Opt Soc Am B 2012; 29: 101-108.

[58] Donati S, Fathi MT. Transition from short-to-long cavity and from self-mixing to chaos in a delayed optic a feedback laser. IEEE J Quantum Elect 2012; 48: 1352-1359.

[59] Priyadarshi S, Pierce I, Hong Y, Shore KA. Optimal operating conditions for external cavity semiconductor laser optical chaos communication system. Semicond Sci Technol 2012; 27: 094002, doi:10.1088/0268-1242/27/9/094002.

[60] Osborne S, Heinricht P, Brandonisio N, Amann A, O'Brie S. Wavelength switching dynamics of two-colour semiconductor lasers with optical injection and feedback. Semicond Sci Technol 2012; 27: 094001, doi:10.1088/0268-1242/27/9/094001.

[61] Mahmouda SWZ, Ahmed M, Hassan AMA. Comprehensive large-signal analyses of RF modulation of vertical cavity surface emitting lasers. Opt Laser Technol 2013; 45: 406-413.

[62] Kechaou K, Grillot F, Provost JG, Thedrez B, Erasme D. Self-injected semiconductor distributed feedback lasers for frequency chirp stabilization. Opt Express 2012; 26062-26074.

[63] Shahverdiev EM, Shore KA. Multiplex chaos synchronization in semiconductor lasers with multiple optoelectronic feedbacks. 2011 Chaotic Dynamics (nlin.CD); Adaptation and Self-Organizing Systems (nlin.AO) 2011; arXiv:0906.4303v2 [nlin.CD].

[64] Li N, Pan W, Luo B, Yan L, Zou X, Xu M, Jiang N. Numerical characterization of time delay signature in chaotic vertical-cavity surface-emitting lasers with optical feedback. Opt Commun 2012; 285: 3837-3848.

[65] Virte M, Panajotov K, Thienpont H, Sciamanna M. Deterministic polarization chaos from a laser diode. Nat Photonics 2013; 7: 60-65.

[66] Argyris A, Syvridis D, Larger L, Annovazzi-Lodi V, Colet P, Fischer I, García-Ojalvo J, Mirasso CR, Pesquera L, Shore KA. Chaos-based communications at high bit rates using commercial fibre-optic links. Nature 2005; 438: 343-346.

[67] McKinney JD, Leaird DE, Hastings AS, Weiner AM, Williams KJ. Optical comb sources and high-resolution optical filtering for measurement of photodiode harmonic distortion. J Lightwave Technol 2010; 28: 1228-1235.

[68] Lee SH, Kim MW, Rim S, Kim CM, Kim JH, Oh KR. Experimental measurement of gain and loss in a microcavity laser. Phys Rev A 2012; 85: 023839; doi:10.1103/PhysRevA.85.023839.

[69] Sciamanna1 M, Virte M, Masoller C, Gavrielides A. Hopf bifurcation to square-wave switching in mutually coupled semiconductor lasers. Phys Rev E 2012; 86: 016218; doi:10.1103/PhysRevE.86.016218.

[70] Romeira B, Javaloyes J, Figueiredo JML, Ironside CN, Cantú HI, Kelly AE. Delayed feedback dynamics of Liénard-type resonant tunneling-photo-detector optoelectronic oscillators. IEEE J Quantum Elect 2013; 49: 31-42.

[71] Lin YS. Theory of stability and bifurcation in a multi-quantum well laser with opto-electronic delayed feedback. Opt Laser Technol 2012; 44: 83-91.

[72] Khursana AHA, Ghalibb BA, Al-Obaidic SJ. Numerical simulation of optical feedback on a quantum dot lasers. Semiconductors 2012; 46: 213-220.

[73] Ling J, Ma J, Zhuang S. Experimental research on profile measurement based on laser optical feedback. Optik 2012; (in press), doi: 10.1016/j.ijleo.2012.05.018.

[74] Hassine L, Toffano Z, Lamnabhi-Lagarrigue F, Destrez A, Birocheau C. Volterra functional series expansions for semiconductor lasers under modulation. IEEE J Quantum Elect 1994; 30: 918-928.

[75] Tucker RS. High-speed modulation of semiconductor lasers. J Lightwave Technol 1985; 3: 1180-1192.

[76] Olshansky R, Hill P, Lanzisa V, Powazinik W. Universal relationship between resonant frequency and damping rate of 1.3 $\mu$m InGaAsP semiconductor laser. Appl Phys Lett 1987; 50: 653-655.